Surface Deposition of Molecular Contaminants in the Mars 2020 Rover Wake

Jason Rabinovitch* and Ira Katz†
Jet Propulsion Laboratory, California Institute of Technology, Pasadena, California, 91109

The Mars 2020 rover has very strict contamination control requirements in order to prepare samples for a potential Mars Sample Return. It is known that the rover will outgas a low-level of molecular contaminant on the surface of Mars, and numerical simulations using STAR-CCM+ are performed in order to predict the magnitude of the contaminant deposition to the Martian surface in the vicinity of the rover. This is done in order to determine whether or not the M2020 rover could self-contaminate a potential sampling site if it were to remain in the same location for a long period of time. Simulations are performed under a variety of surface conditions, and it is determined that the predicted level of molecular contaminant deposition to the surface near the rover will not be a significant factor in the overall sample contamination budget.

Nomenclature

D	=	Binary diffusion coefficient, m^2/s
$\hat{\mathbf{i}}, \hat{\mathbf{j}}, \hat{\mathbf{k}}$	=	Unit vectors in the x, y, and z directions, respectively
L	=	Characteristic length-scale, m
$M2020$	=	Mars 2020
$MMRTG$	=	Multi-Mission Radioisotope Thermoelectric Generator
MSL	=	Mars Science Laboratory
μ	=	Dynamic viscosity, kg/(m·s)
$\tilde{\mu}$	=	Turbulent dynamic viscosity, kg/(m·s)
ν	=	Kinematic viscosity, m^2/s
ϕ	=	Passive scalar volume fraction
$\tilde{Pr}$	=	Turbulent Prandtl number
$RANS$	=	Reynolds-Averaged Navier-Stokes
Re	=	Reynolds number
ρ	=	Gas density, kg/m^3
Sc	=	Schmidt number
$\tilde{Sc}$	=	Turbulent Schmidt number
θ	=	Wind direction
TOC	=	Total Organic Carbon
U	=	Magnitude of characteristic free-stream velocity, m/s
WEB	=	Warm Electronics Bay
x_v, y_v	=	x and y coordinates of centroid of the two rover vents, m
z_g	=	z coordinate of ground plane, m

I. Introduction

One of the primary scientific objectives of the next NASA planned Mars rover, Mars 2020 (M2020), is to acquire and cache Martian surface samples for potential Mars sample return.* For both scientific integrity and planetary protection reasons, acceptable contamination levels for the acquired samples are lower than any previous Mars mission [1]. Level one requirements state that the Total Organic Carbon (TOC) level of contamination per sample tube shall be less

*Engineer, Entry, Descent, & Landing and Formulation Group, 4800 Oak Grove Drive, M/S: T1708-112, Member AIAA.
†Technologist, Principal, Propulsion, Thermal, & Material Systems Group, 4800 Oak Grove Drive, M/S: 125-109, Senior Member AIAA.
*https://mars.nasa.gov/mars2020/, accessed 10/20/2017.

than 150 ng, and each sample tube has a cross-sectional area of ~ 1 cm^2. This contamination requirement represents an integrated quantity that includes contaminant deposition during spacecraft fabrication, assembly, launch, cruise, surface operations, and then a return trip to earth. As such, even potential molecular contamination of sampling sites due to the proximity of the rover must be considered, and this work presents results from modeling possible molecular contamination of a drill site due to contaminants outgassing from the M2020 Rover during surface operations on Mars.

This paper provides an overview of the operational scenario of interest for this work, discuss the modeling approach and assumptions used, and then provides a discussion of the simulation results.

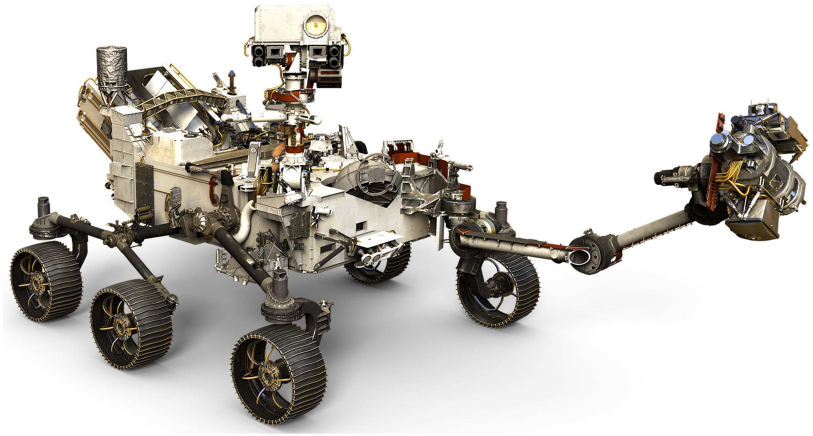

Fig. 1 Mars 2020 Rover rendering. Photo credit: NASA (https://mars.nasa.gov/mars2020/mission/rover/, accessed 10/20/2017.)

II. Background

Primarily due to warm electronics located inside of the rover in the Warm Electronics Bay (WEB), some amount of material outgassing is expected to occur while the rover operates on Mars. Based on tests performed on Earth, an expected molecular outgassing rate from the rover is known. In addition, strict design requirements are levied on the rover to limit the maximum amount of outgassing that will occur. The detailed tracking of possible contaminants is standard for Mars surface missions, and an example analysis for the Mars Science Laboratory (MSL) mission can be found in [2].

Figure 2 depicts the basic operational scenario of interest for this work. When the rover is operating on Mars, molecular contaminants generated inside of the rover are expected to exit the rover chassis through two vents - one located on the aft end of the rover, and one located on the port side of the rover. Once the contaminants have left the confines of the rover chassis, they are expected to advect away from the rover due to surface winds, and to diffuse due to concentration gradients. Depending on wind direction and location of the rover, it is therefore possible for molecular contaminants to be deposited on a possible sampling site. Martian surface winds have been characterized during previous missions (for example, see [3–5]), and experimentally measured wind speeds will serve as the foundation for initial conditions for this study.

If deemed necessary, the M2020 Rover will loiter up to 100 sols near a potential sampling site of interest. It is assumed that the rover turret would be in the vicinity of the potential sampling site so that the instruments housed on the M2020 turret can be used to investigate the side of interest. Specifically, flight rules state that with the rover turret within 0.5 m of a potential coring site, the rover could possibility remain in the same location for up to 50 Martial sols, and up to 100 Martian sols for the turret within 10 m of a potential coring target. This operational configuration is the basis for the assumed geometry of the simulations presented in the following sections, where the wind primarily flows over the back of the rover towards the deployed turret, which convects the contaminant closer to a possible sampling site, as shown in Fig. 2.

Based on the predicted level of surface contamination from this work, it will be decided whether or not an operations requirement will have to be created to limit how long the rover can remain close to a possible sampling location before the sampling site is deemed to have been unacceptably contaminated by the rover.

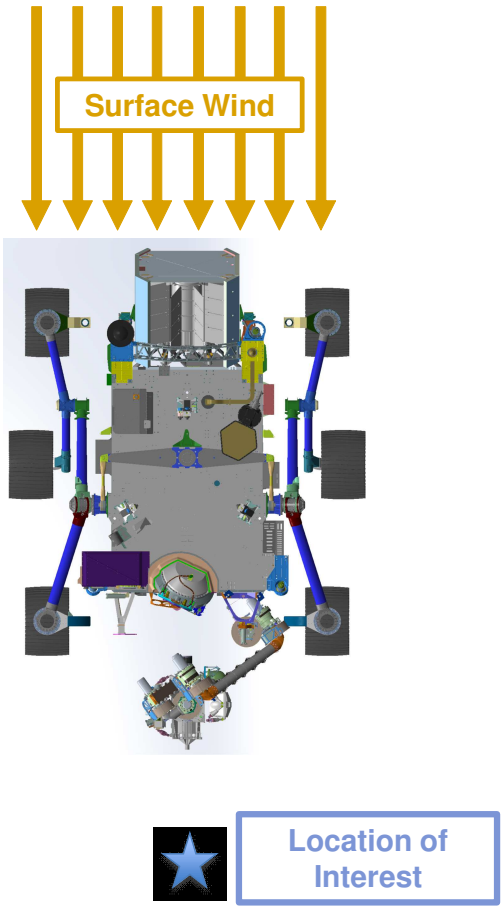

Fig. 2 General schematic of contamination scenario considered. In this schematic, a possible sampling site is directly downstream of the rover, though this work looks at the predicted contamination deposited in a large area close to the rover and not just directly downstream, and also varies the direction of the surface wind.

III. Numerical Model

The subject of passive scalar advection/diffusion in turbulent wakes is a field that contains a rich set of complex physics, and has been studied with great scientific rigor in the past (for example, see [6–9]). However, in this work, an engineering approximation is required to predict the amount of contaminant that will be deposited on the Martian surface in the vicinity of the M2020 rover. Ie, factors of ~10 in overall mass deposition are quite significant, but factors of ~ 2 are likely insignificant assuming the predicted mass deposition to the surface is small enough. Furthermore, the complex geometry of the rover itself and the asymmetric locations of the vents that act as sources for the contaminant (Fig. 3) introduce geometrical complications that are rarely considered in canonical research problems.

With these considerations in mind, the commercial CFD package STAR-CCM+[†] is used for this work. A steady state incompressible (density variations only due to temperature) coupled flow and energy solver is used for this work. The flowfield is solved concurrently with an advection/diffusion equation to model the transport of molecular contaminants near the rover, which is modeled numerically as a passive scalar. In order to account for small oscillations after convergence is achieved, results shown in this work have been averaged over many iterations. Simple verification problems were solved originally (flow around a sphere and 1D unsteady diffusion) in order to ensure that the numerical methods were producing expected results for canonical problems. This section provides an overview of the numerical modeling approach used.

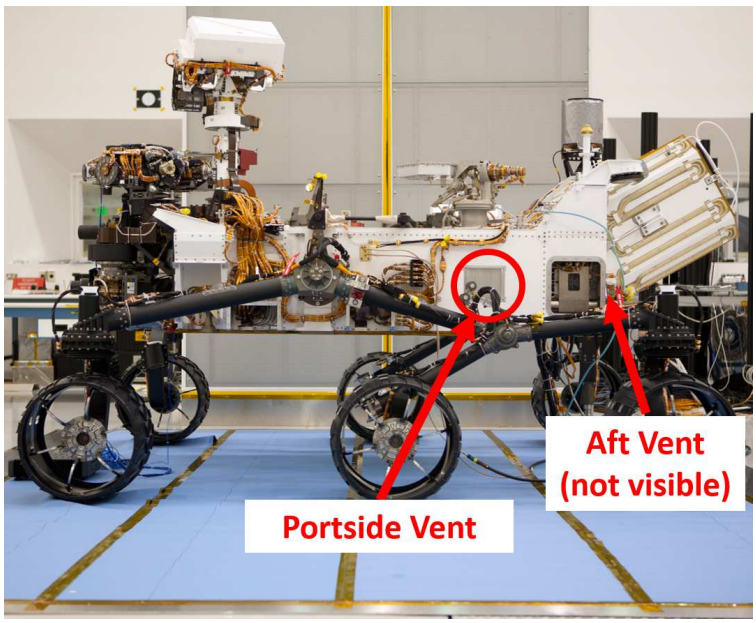

Fig. 3 Image of the MSL rover taken at NASA/JPL. The portside vent can clearly be seen, and the aft vent is located on the back of the rover, which is not visible in the image. These two vents are considered to be the only sources of a passive scalar for this work.

A. Numerical Domain

Figure 4 shows a schematic of the numerical domain used in this work. Standard M2020 spacecraft coordinates are used, such that the x-axis runs from the front to the back of the rover, with the aft end of the rover located on the $-x$ side, and the front of the rover (where the deployed turret is located) on the $+x$ side (Fig. 5). The origin of the coordinate system is located roughly at the centroid of the rover. A cylindrical domain is used, with the $-x$ curved surface being the inlet, and the $+x$ surface being the outlet. The ground plane, z_g, is located at $z_g = 1.13$ m, with the z-axis oriented in the direction of gravity. The y-axis is chosen to define a standard right-handed set of orthogonal coordinates. A top-plane is also included, though not shown in Fig 4. Table 1 gives a summary of the numerical boundary conditions applied to the domain surfaces (see section III.B for a description of the rover boundary conditions used).

The numerical domain has a diameter of 50 m, which corresponds to $\sim$ 25 characteristic rover lengths, as the M2020 rover is $\sim$ 2 m x 2 m x 2 m. The height of the domain is 15 m. Therefore, the min/max spatial coordinates in the domain are x: [-25.0, 25.0] m, y: [-25.00, 25.00] m, and z: [-13.87, 1.130] m. This relatively large domain is used in order to minimize the effect that the boundaries will have on the flow field near the rover.

Table 1 Summary of numerical boundary conditions applied.

Surface	STAR-CCM+ Boundary	Parameters
Inlet	Velocity Inlet	Flow inlet with user specified velocity profile (see Sec. III.D)
Outlet	Pressure Outlet	Outlet surface with extrapolated backflow properties when needed
Ground Plane	Wall	No-slip adiabatic surface with a passive scalar concentration of 0
Top Plane	Pressure Outlet	Outlet surface with extrapolated backflow properties when needed

B. Rover Geometry

A simplified M2020 rover model (Fig. 5) is used in order to retain all major components of the M2020 rover, yet reduce the amount of geometric complexity present so that the model is still numerically tractable. The majority of the

[†] https://mdx.plm.automation.siemens.com/star-ccm-plus, accessed 5/1/2018

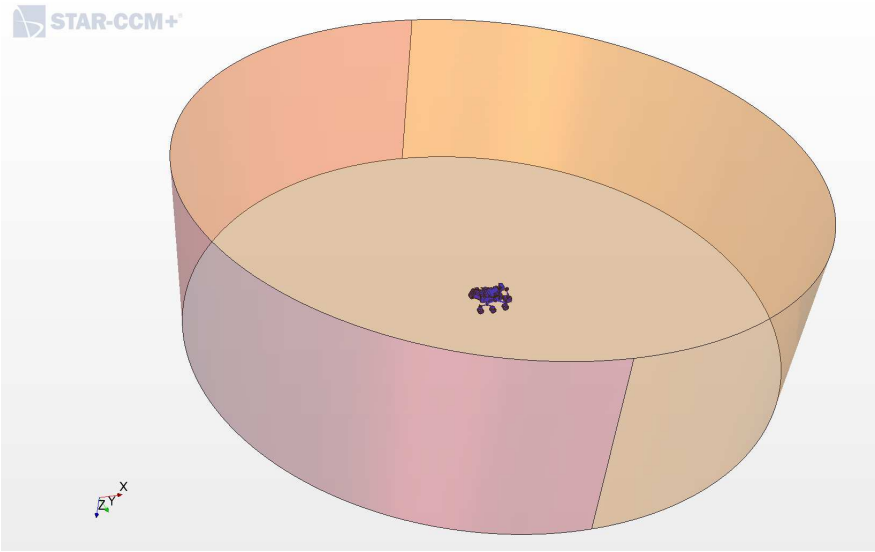

Fig. 4 Numerical domain used in this work. A 50 m diameter cylindrical domain is used in order to ensure that there is an adequate distance between the rover and domain boundary.

surfaces of the rover are defined to be no-slip adiabatic walls with a specified passive scalar flux of zero. However, as M2020 is powered by a Multi-Mission Radioisotope Thermoelectric Generator (MMRTG), which converts heat into electrical power, some surfaces on the rover are expected to be hot, and these are discussed in Sec. III.B.1. The two vents, which are assumed to be the only sources of contamination in this work, are discussed in Sec. III.B.2.

1. Radioisotope Thermoelectric Generator (RTG) Hot Surface

The M2020 Rover will use the same MMRTG power source as the MSL Rover, which provides an electrical power output of approximately 110 W [10]. While the temperature of the MMRTG is expected to vary based on local temperature (which can be landing site dependent), wind speed, di-urnal, and seasonal variation, etc., in this work a constant isothermal temperature is assumed for the MMRTG cylinder and fins, as illustrated by Fig. 6. While MSL flight data [11, 12] shows that MMRTG temperatures can vary significantly, a conservative bounding lower temperature of 115°C is chosen, which is well below any MSL observed temperatures. As the hot MMRTG induces a buoyant gas plume, this causes streamlines around the rover to move away from the Martian surface, which in turn convects possible

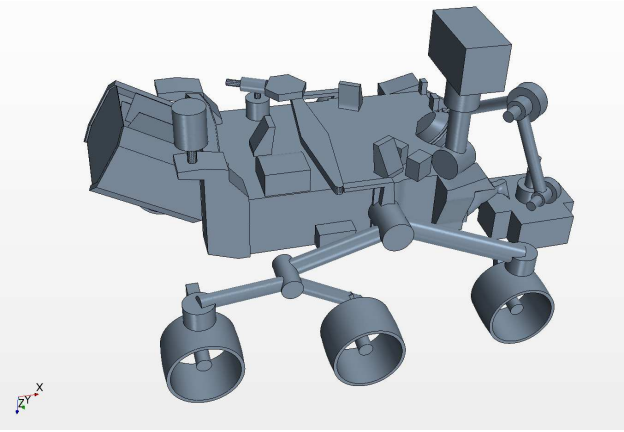

Fig. 5 Simplified M2020 rover model used for this work. All major components have been retained, though some of the small features seen in Fig. 1 and 3 have been ignored for computational considerations.

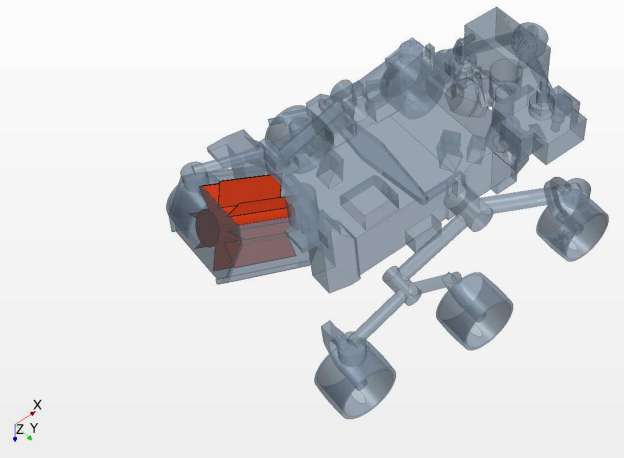

Fig. 6 Simplified M2020 rover model with MMRTG surfaces (115°C) shown in red. The rest of the rover model is made translucent to show the 3D nature of the MMRTG.

contaminants away from the surface. Therefore, the hotter the MMRTG is, a lower amount of contamination will be deposited on the surface. Conversely, not accounting for MMRTG induced buoyancy could cause an nonphysical over-prediction of the amount of contaminant expected to be deposited on the Martian surface in the vicinity of the rover.

2. Contamination Sources

As previously discussed, the WEB is the primary source of contamination considered in this study. There is a M2020 requirement (that is verified via test) that the outgassing through the vents shall be less than 100 ng/(cm^2·hour). This worst-case value is used in this study, and worst-case outgassing is expected to occur when Mars surface temperatures, and subsequently WEB temperatures are high (relative to average Mars surface temperatures). All components of the M2020 Rover will go through bakeout cycles before launch in order to significantly reduce the amount of contaminant that can outgas on the surface of Mars. Because of this, it is assumed that only larger hydrocarbons outgas on Mars, as smaller molecules would have been depleted during earlier contamination bakeout processes.

Using transport properties given in [13], the binary diffusion coefficient (D) can be estimated for non-polar gases as a function of temperature and pressure. A conservatively small characteristic n-alkane of C_5H_{12} is chosen, which, for the conditions used in this work, gives a binary diffusion coefficient of $6 \cdot 10^{-4}$ m^2/s into CO_2. Temperature dependence of the binary diffusion coefficient is not accounted for in this work, as a large temperature gradient in the gas only exists in a small region. The contaminant is assumed to leave the rover chassis through two vents, shown for the numerical model in Fig. 7.

Due to the relatively low concentration levels of this contaminant in the flow, the contaminant is modeled numerically as a passive scalar (with a volume fraction of ϕ), i.e., assuming that the contaminant does not alter the bulk atmospheric gas properties in a significant manner, so that a multi-component gas mixture does not have to modeled numerically.

C. Meshes

The computational mesh used in this study is generated primarily to try to resolve the ground plane boundary layer, boundary layers over the rover surfaces, and the wake region behind the rover. The STAR-CCM+ polyhedral meshing algorithm is used in conjunction with a prism layer algorithm to generate all meshes used in this work. With the large numerical domain shown in Fig. 4, only two meshes are used to perform a pseudo-mesh refinement study. The first mesh contains $\sim 9.6 \cdot 10^6$ cells and the second, more refined mesh, contains $\sim 2.6 \cdot 10^7$ cells. For a characteristic free-stream velocity of 1.4 m/s no significant difference in mass flux of contaminant to the ground is observed between the two meshes. However, as will be discussed in Sec. IV.A, in order to accommodate an increased free-stream velocity, and for consistency when comparing results, all results presented in later sections are generated using the most refined mesh. The refined rover surface mesh used is shown in Fig. 8, and the entire domain mesh with a center-plane cut is shown in Fig. 9.

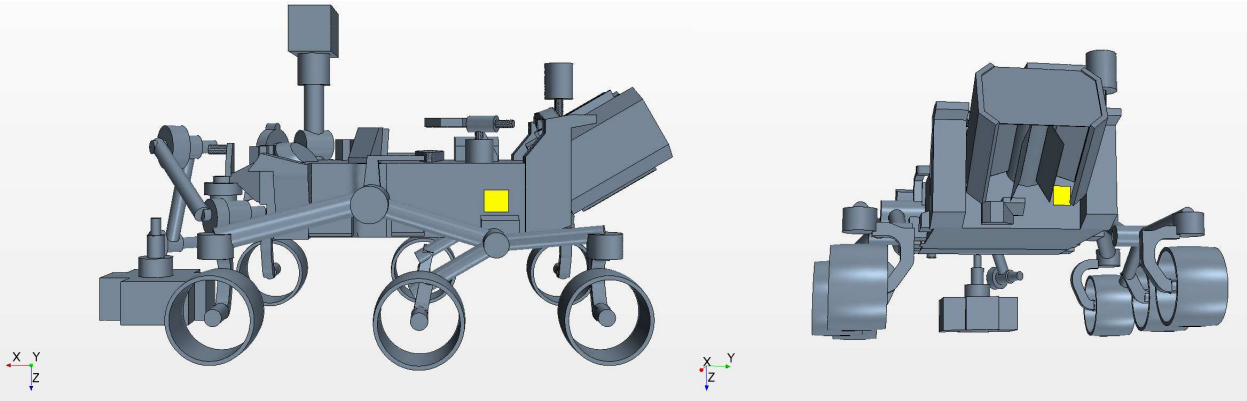

Fig. 7 Simplified M2020 rover model with vent surfaces shown in yellow (left: port vent, right: aft vent). These surfaces are contanimant (passive scalar) sources in the numerical simulations.

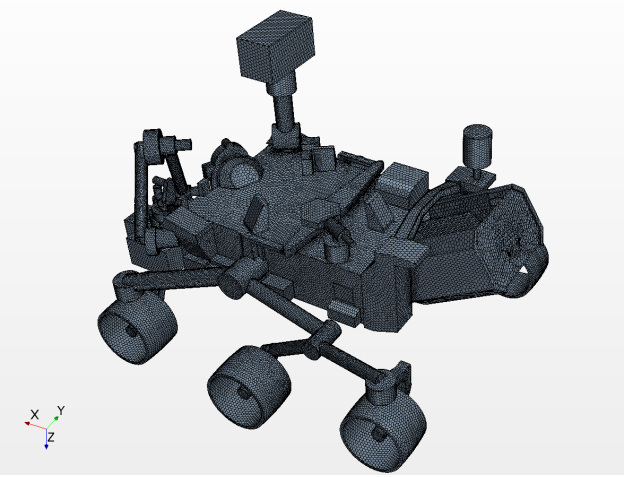

Fig. 8 Simplified M2020 rover model with the refined surface mesh shown.

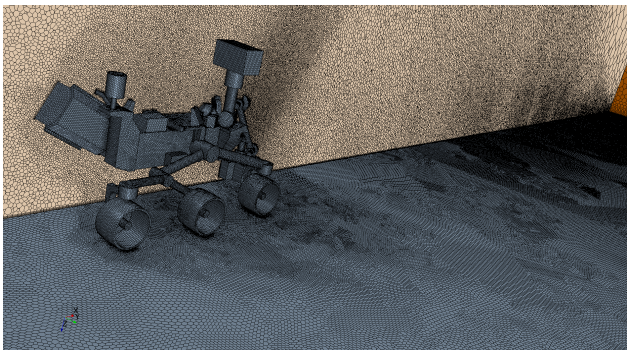

Fig. 9 Snapshot of overall domain with surface meshes shown on the rover, ground plane, domain outlet, and a center-plane section cut.

D. Initial Conditions

The physical scenario of interest for this work is a Martian surface wind blowing over the M2020 rover. In order to stay consistent with the assumed high WEB contaminant outgassing values, a relatively high ambient Mars temperature of 10°C (283 K) is assumed for this work. This high temperature also reduces the temperature difference between the free-stream and hot MMRTG surfaces. A free-stream pressure of 1070 Pa is assumed, and for simplicity, a 100% CO_2 gas mixture is assumed. Using the ideal gas law, this results in a density of 0.02 kg/m^3. Based on previous measurements (for example [14]) CO_2 is the primary constituent in the Mars atmosphere ($\sim$ 96% by volume). Neglecting the other trace species in this work will not have a significant affect on the quantities of interest being investigated as the gas bulk mixture properties are dominated by the CO_2 content. The standard Sutherland's law is assumed for dynamic viscosity and gas thermal conductivity, and a polynomial fit based on temperature is used for gas specific heat. The free-stream value for dynamic viscosity is $1.76 \cdot 10^{-5}$ Pa-s. Mars gravity is assumed to be 3.711 m/s^2, and due to the reference frame chosen for this work, gravity acts in the $+z$ direction.

A simple logarithmic wind boundary layer profile is assumed for this work with values extracted from viking wind data.[‡] An inlet velocity profile of

$$U(z) = U(z_{ref}) \frac{\log(|z - z_g|/z_0)}{\log(z_{ref}/z_0)} \tag{1}$$

is used, where $U(z)$ is the magnitude of the free-stream velocity, z_{ref} is a characteristic measurement height based on the Viking lander instrument suite (1.6 m), and z_0 is the surface roughness scale height, assumed to be 0.01 m in this work. As the wind speed on Mars is not constant, a variety of different values for $U(z_{ref})$ can be chosen.

Two different values of $U(z_{ref})$ are used in this work: 1.4 m/s and 5.0 m/s. 1.4 m/s corresponds to a $\sim$ 10%tile surface wind, and 5.0 m/s corresponds to a $\sim$ 65%tile wind based on Viking data. Depending on how far away from a potential sampling site the rover is, a low-speed or high-speed wind could provide a larger amount of contamination deposition to the area of interest. The direction of the free-stream is also varied in this work, thought it is primarily aligned with the x-axis. The angle of attack (AoA) is taken to be in the $x - y$ plane for this work (roll plane of the rover), with a positive AoA defined to be a counter-clockwise rotation from the x-axis to the y-axis. With a positive angle of attack, the port-side vent moves closer to the stagnation point of the flow, and with a negative angle of attack the port-side vent moves closer to being in the rover wake. A summary of the initial conditions used for the flow is shown in Table 2.

E. Turbulence Modeling

For characteristic velocities (U) of 1.4 m/s and 5.0 m/s, a characteristic length (L) of 2 m, a kinematic viscosity (ν) of $8.8 \cdot 10^{-4}$ m^2/s, the predicted Reynolds numbers ($Re = \frac{U \cdot L}{\nu}$) are $Re \simeq 3000$ and $Re \simeq 1000$ for the two different characteristic free-stream velocities, respectively. This puts the flow in a regime where an unsteady turbulent vortex street is expected to be observed in the wake [15]. It should be noted that the local Re around different individual geometrical features is likely to be lower, i.e., if the characteristic lengthscale was chosen to be the mast diameter. However, these lower Re areas are still expected to generate an unsteady vortex street, though the flow may be in a

[‡] http://www-k12.atmos.washington.edu/k12/resources/mars_data-information/data.html, accessed 5/3/2018.

Table 2 Summary of initial fluid conditions used.

Property	Value(s)
Temperature (K)	283
Pressure (Pa)	1070
Density (kg/m^3)	0.02
$U(z_{ref})$ (m/s)	1.4, 5.0
AoA (°)	0°, ±5°, ±15°, ±30°

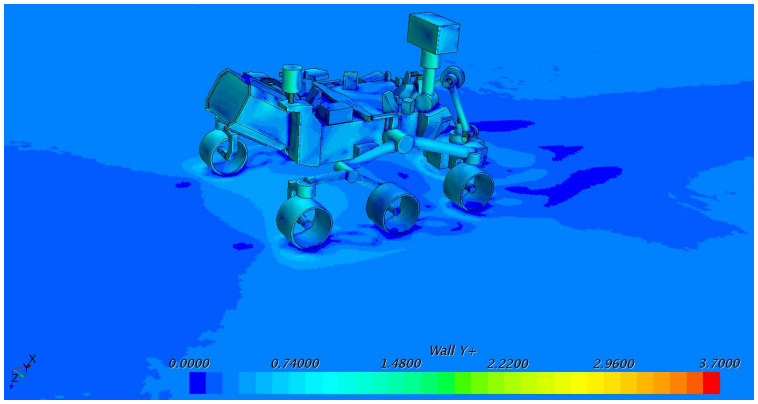

Fig. 10 Contour plot showing calculated y^+ values on the ground plane and rover surface for $U(z_{ref}) = 1.4$ m/s, and 0° angle of attack.

transitional state).

Due to the engineering nature of this problem, both steady-state laminar and turbulent simulations were completed for the same initial conditions. Both the Realizable K-Epsilon Two-Layer Reynolds-Averaged Navier-Stokes (RANS) turbulence model and the SST(Menter) K-Omega RANS turbulence models were used in preliminary simulations with default coefficients, with meshes resolving $y^+ \simeq 1$. Simulations with the K-Epsilon model were found to predict the largest amount of contaminant mass deposition to the surface, so this model was used for all results presented in Sec. IV. Constant turbulent Prandtl ($\tilde{Pr}$) and Schmidt ($\tilde{Sc}$) numbers of 0.9 are assumed in the flow.

IV. Results

This section provides a summary of results generated to date based on the initial conditions discussed in the previous section. Rover surface y^+ will be presented to give a quantitative measure of the mesh resolution attained in this study, and then both flow field properties and contaminant mass deposition results are showed.

A. Mesh Size and Computations

Figures 10 and 11 show calculated y^+ values on the ground plane and rover surface for the refined mesh ($\sim 2.6 \cdot 10^7$ cells) for characteristic free-stream velocities of 1.4 m/s and 5.0 m/s, respectively. An AoA of 0° is used in both of these cases. The maximum y^+ values observed on the rover are 1.9 and 3.7 for the two different free-stream velocities. y^+ values > 1 are generally only see in local stagnation regions and in areas where flow separation is expected to occur, which gives confidence in the mesh resolution used. Computations are run locally at JPL using 240 cores on the Zodiac cluster. After 1,000 iterations (when a converged solution is reached), the results presented below are averaged over 9,000 additional iterations. While less relevant when RANS turbulence models are being used, with preliminary laminar simulations, oscillations were observed in the solution (likely due to unsteady vortex shedding), and an average solution over several flow cycles was desired in order to give a relevant averaged result. These oscillations in residuals are generally not seen once a turbulence model is enabled.

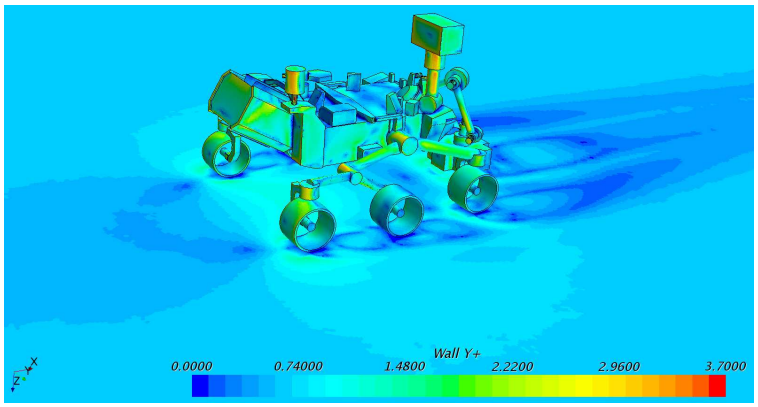

Fig. 11 Contour plot showing calculated y^+ values on the ground plane and rover surface for $U(z_{ref}) = 5.0$ m/s, and 0° angle of attack.

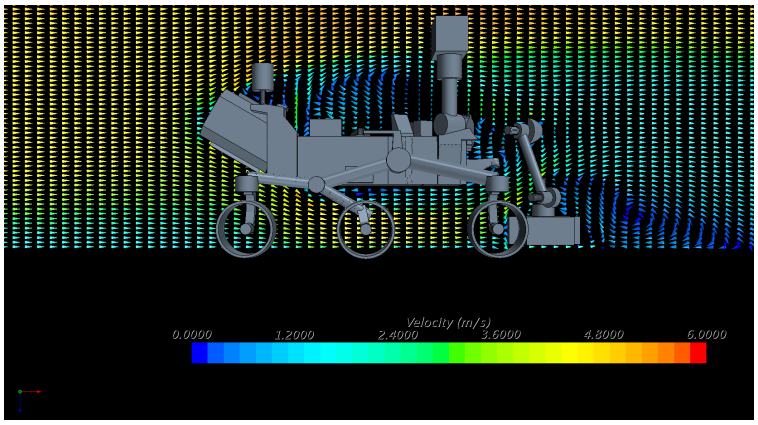

Fig. 12 Mean velocity vectors colored by velocity magnitude along the center-plane of the domain for $AoA = 0^\circ$ and $U(z_{ref}) = 5.0$ m/s. Two primary re-circulation regions above the rover deck and downstream of the turret can be seen.

B. Flow Field

For brevity, this section only shows sample results for a free-stream characteristic velocity of 5.0 m/s, and a 0° AoA. Figure 12 shows velocity vectors colored by velocity magnitude along the center-plane of the domain which means that the three-dimensional nature of the flow field is not shown. As expected, re-circulation zones are visible near the rover top-deck and behind the deployed turret. Figure 13 shows the relatively small region where the gas temperature has increased due to the hot RTG surfaces in the simulation. A cut of the center-plane of the domain is shown where the gas temperature is between 284 K and 388 K. The hot MMRTG surface is shown in red.

Qualitatively, varying the angle of attack of the flow and flow velocity does not change the major features observed in the flow solution (standard bluff body flow phenomena). However, and this will be discussed in more detail in the next section, due to the complex geometry of the rover and the location of the vents, the overall deposition of contaminant to the surface is sensitive to streamlines near the vents traveling either under the rover chassis or over the rover top-deck. If these streamlines, which generally correspond to regions of the flow with a relatively high concentration of contaminant, travel beneath the rover, then the contamination is convected closer to the ground plane, which will increase the mass deposition levels observed in the rover wake.

C. Contamination Concentrations and Mass Deposition

The quantity of interest in this study is the mass flux of the passive scalar (molecular contaminant) to the surface. As discussed previously, the ground plane has a boundary condition set to 0 concentration of passive scalar, which means that no contaminant accumulates on the surface. The magnitude of the diffusion mass flux to the surface ($\dot{m}$) is

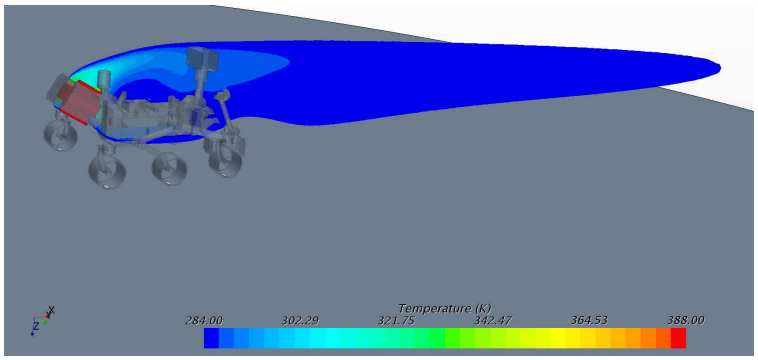

Fig. 13 Gas temperature along the center-plane of the numerical domain for $AoA = 0°$ and $U(z_{ref}) = 5.0$ m/s. The gas termperature contour is clipped so that only areas of the flow with 284 K$\leq T \leq$ 388 K are shown. The hot RTG surface is shown as well.

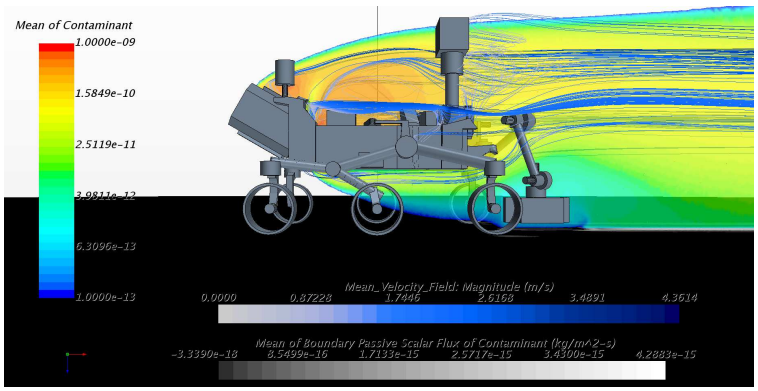

Fig. 14 Simulation results for $AoA = 0°$ and $U(z_{ref}) = 5.0$ m/s. Streamlines eminating from the rover vents and contaminant concentration along the center-plane is shown. It is possible to see some of the streamlines which travel under the rover and closer to the surface.

desired, which can be calculated from

$$\dot{m} = -\left(\frac{\mu}{Sc} + \frac{\tilde{\mu}}{\tilde{Sc}}\right)\nabla\phi \cdot \hat{\mathbf{k}}, \tag{2}$$

where μ is the dynamic viscosity, $\tilde{\mu}$ is the turbulent viscosity, and $\hat{\mathbf{k}}$ is the unit vector in the z direction. The mass flux due to convection is 0 due to the ground plane being a no-slip/no-penetration wall, and in the coordinate system used, $\dot{m}$ should be positive when mass is deposited on the surface. The mass diffusion flux has standard units of kg/(m^2·s), though for the majority of the rest of this work, results will be presented using units of ng/(cm^2·sol) in order for comparisons relevant to M2020 timescales and length scales to be made in a simple manner. One Martian sol (day) is taken to be 24 hours, 39 minutes, and 35.244 seconds. Due due to low value of the binary diffusion coefficient of the contaminant under Mars conditions, turbulent mixing drives the evolution of the contaminant field, and not pure mass diffusion.

Figures 14 and 15 show streamlines emanating from the contaminant vent surfaces as well as the concentration of the contaminant along the center-plane of the domain for the 5 m/s characteristic free-stream velocity with 0° angle of attack. The ground plane is colored by predicted mass deposition to the surface. Some streamlines travel beneath the rover which indicates that some of the contaminant is initially convected close to the surface, which causes an increased amount of contaminant to be deposited to the surface.

Sample mass deposition contour plots for a characteristic free-stream velocity of 5 m/s, and wind angles of -30°, 0°, and 30°, are shown in Figs. 16–18. STAR-CCM+ results generated on an unstructured grid on linearly interpolated onto a cartesian grid with equal spacing with 501 points in each of the x and y directions. Dashed circles are plotted at a radius of 5 m and 10 m from the center of the rover for scale. The direction of the free-stream is also shown, and

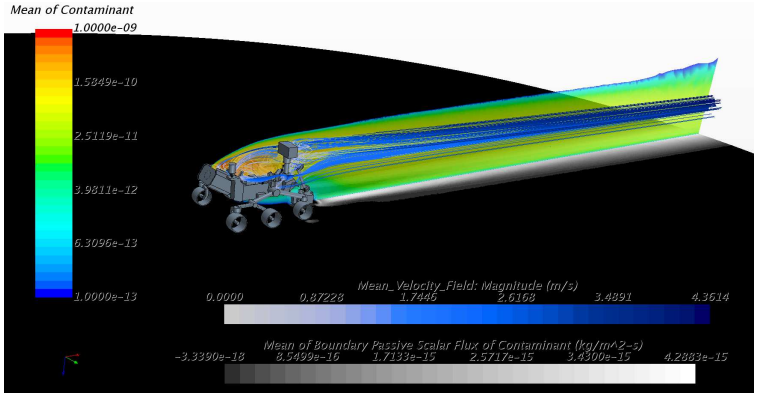

Fig. 15 Simulation results for $AoA = 0°$ and $U(z_{ref}) = 5.0$ m/s. Streamlines eminating from the rover vents and contaminant concentration along the center-plane is shown. A relatively small growth in the vertical direction of the contaminant profile is seen downstream due to the relatively small amount of molecular diffusion occuring before the flow exits the domain.

an approximate rover outline (with vents indicated) is shown in green.

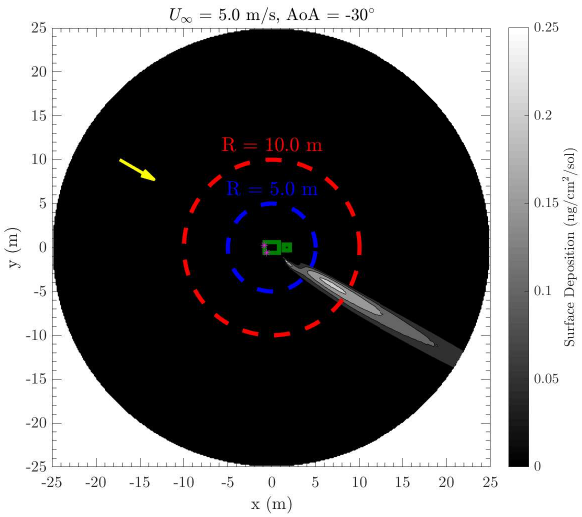

Fig. 16 Predicted contaminant surface mass deposition contour plot for $AoA = -30°$ and $U(z_{ref}) = 5.0$ m/s. The free-stream direction is shown by the yellow arrow, and an approximate outline of the rover and turret is shown in green (with vents noted). Circles showing 5 m and 10 m distances from the origin.

In order to compare the effect of free-stream angle of attack on the two wind speeds considered, Figs. 19 and 20 show integrated mass deposition (not flux) values as a function of radius (calculated to ensure conservation of mass in the domain). Radius is defined as the distance to the origin based on the centroid of the two vents ($r = \sqrt{(x - x_c)^2 + (y - y_c)^2}$). High angle of attack flows (both in the positive and negative direction) generally have the highest total mass depositions to the surface. This is primarily attributed to the location of the port vent, as for the $AoA = \pm 30°$ wind directions, the port-side vent is located closer to either the wake or the stagnation region of the rover (compared to the 0° wind direction). With this flow/rover alignment, the port-vent streamlines, and therefore contaminant, are convected closer to the ground, which ends up increasing the level of mass deposition for these wind angles.

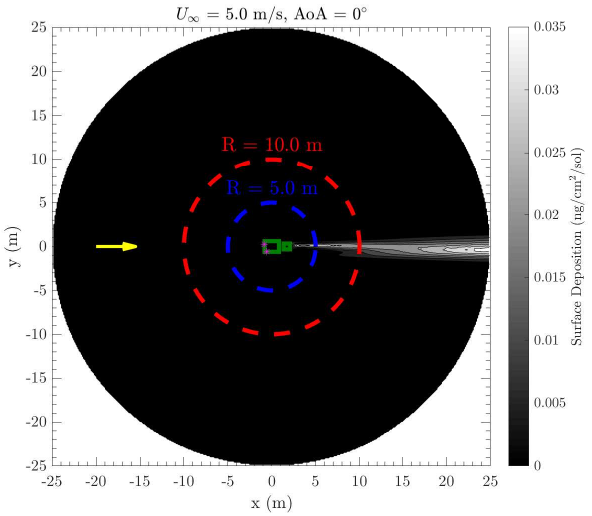

Fig. 17 Predicted contaminant surface mass deposition contour plot for $AoA = 0°$ and $U(z_{ref}) = 5.0$ m/s. The free-stream direction is shown by the yellow arrow, and an approximate outline of the rover and turret is shown in green (with vents noted). Circles showing 5 m and 10 m distances from the origin are shown for scale.

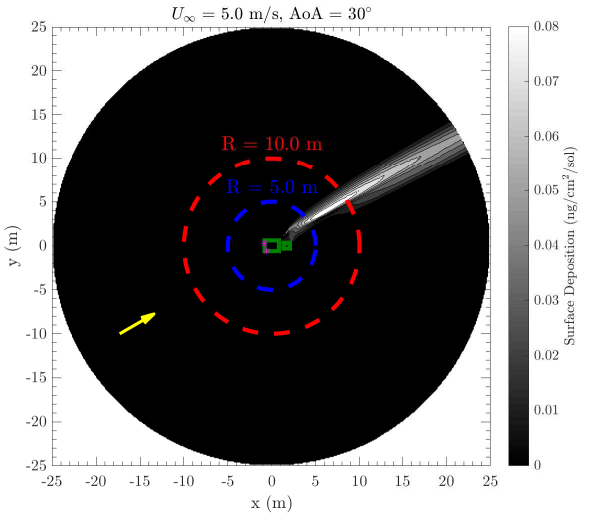

Fig. 18 Predicted contaminant surface mass deposition contour plot for $AoA = 30°$ and $U(z_{ref}) = 5.0$ m/s. The free-stream direction is shown by the yellow arrow, and an approximate outline of the rover and turret is shown in green (with vents noted). Circles showing 5 m and 10 m distances from the origin are shown for scale.

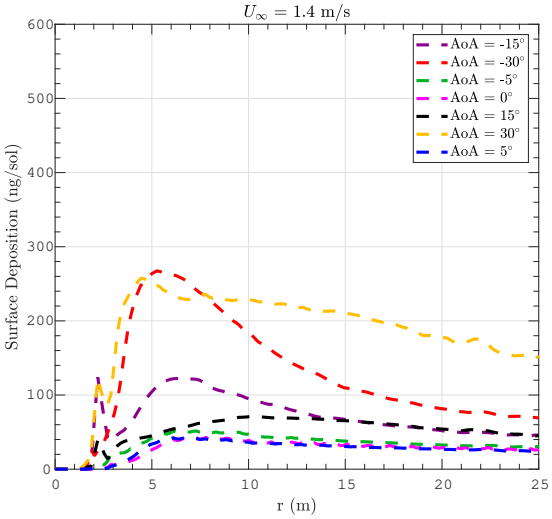

Fig. 19 Integrated contaminant deposition profiles as a function of radius for $U(z_{ref})$ = 1.4 m/s.

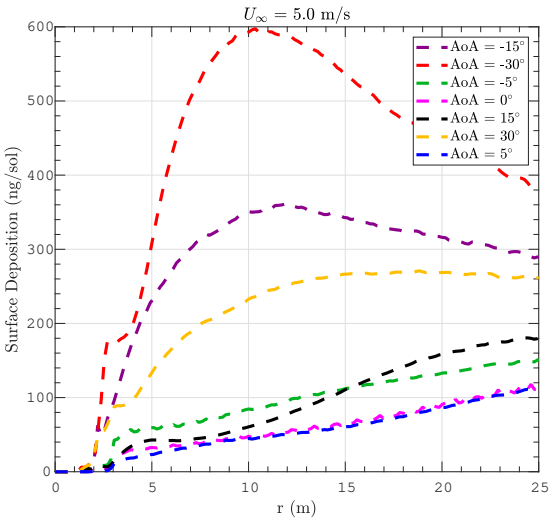

Fig. 20 Integrated contaminant deposition profiles as a function of radius for $U(z_{ref})$ = 5.0 m/s.

D. Spatial Averaging

As shown in [5], MSL has measured significant variance in both wind direction and speed throughout its mission thus far. The simulations presented so far have only been for discrete wind directions and velocities. In order to evaluate the potential contamination risk to a drill site due to the M2020 rover loitering in a single location, timescales on the order of 50 or 100 sols are of interest. This implies that some spatial averaging of the results presented in the previous section should be performed in order to account for the constantly changing Martian surface winds.

The wind environment that the M2020 rover will experience is expected to influenced by many factors, including (but not limited to) seasonal variations, diurnal effects, and geographic effects (both depending on landing site selection, and local terrain features). Due to impracticality of trying to model all of these complex phenomena, a simplified approach is taken.

Wind direction variability is modeled using a normal distribution with a probability density given by

$$f(\theta) = \frac{1}{\sqrt{2\pi\sigma^2}} e^{-\frac{(\theta-\xi)^2}{2\sigma^2}}, \tag{3}$$

where θ is the wind direction, ξ is the mean wind angle, and σ is the standard deviation of the wind direction in degrees. While data in [5] shows a relatively large angle variability in wind direction, here a conservative standard deviation of 15° is assumed.

Discrete numerical results now need to be spatially averaged while still conserving mass from the original simulation results. The algorithm is first described assuming only one numerical simulation at θ_o has been completed, and then will be extended to incorporate results from multiple numerical at multiple angles. θ is linearly discretized where $\theta = [\theta_1, \theta_2, ..., \theta_i, ..., \theta_{n-1}, \theta_n]$, where $n = 1000$, $\theta_1 = \xi - 6\sigma$ and $\theta_n = \xi + 6\sigma$. In order to enforce discrete mass conservation, a numerical weighting coefficient, ψ, is used to ensure $\sum_{i=1}^{n} \psi f(\theta_i) = 1$.

Let $\dot{m}_{n,\theta}(x, y)$ correspond to numerical results for a wind angle of θ linearly interpolated onto a cartesian mesh, still with units of ng/(cm^2·sol). Let $\bar{m}_{\xi,\sigma}(x, y)$ correspond to the averaged contaminant mass flux field for a mean wind angle of ξ and a wind direction standard deviation of σ. Therefore, a spatially averaged contaminant deposition field can be represented by

$$\bar{m}_{\xi,\sigma}(x, y) = \sum_{i=1}^{n} \psi f(\theta_i) \dot{m}_{\theta_i}(x, y). \tag{4}$$

However, in this example, numerical results are only available for $\theta = \theta_o$, ie $\dot{m}_{n,\theta_o}(x, y)$. To account for this, $\dot{m}_{\theta_i}(x, y)$ is calculated by a solid-body rotation of the original $\dot{m}_{n,\theta_o}(x, y)$ solution by a rotation angle, θ_r, of $\theta_r = \theta_i - \theta_o$. With $x = rcos(\theta)$ and $y = rsin(\theta)$, then $\dot{m}_{\theta_i}(x, y) = \dot{m}_{n,\theta_o}\left(cos(\theta_r)x + sin(\theta_r)y, -sin(\theta_r)x + cos(\theta_r)y\right)$ Numerically, the rotated contaminant mass deposition field is project back onto the original cartesian mesh using 2D linear interpolation.

As multiple numerical simulations have been completed, it is possible to combine these results for a given θ_i. For example, assume that numerical simulations have been completed at angles θ_α and θ_β, and $\theta_\alpha < \theta_i < \theta_\beta$. In this scenario, $\dot{m}_{n,\theta_i}(x, y)$ is calculated by rotating $\dot{m}_{n,\alpha}(x, y)$ by $\theta_r = \theta_i - \theta_\alpha$ and by rotating $\dot{m}_{n,\beta}(x, y)$ by $\theta_r = \theta_i - \theta_\beta$ and the summing the two resulting rotated contaminant mass flux fields using appropriate weighting coefficients based on a linear interpolation in θ. If θ_i is outside of the range of numerical simulations completed ($\theta_i < -30°$ or $\theta_i > 30°$ for this study), then no linear interpolation is used, and the numerical results with $\theta = \pm 30$ are rotated accordingly. With this methodology simulations with differing characteristic free-stream velocities are analyzed separately.

Figures 21– 26 show this method for a characteristic free-stream velocity of 1.4 m/s, $\xi = [-30°, 0°, 30°]$, and $\sigma = 15°$, and results for a characteristic free-stream velocity of 5.0 m/s, once again with $\xi = [-30°, 0°, 30°]$, and $\sigma = 15°$.

V. Discussion and Future Work

Even with the conservative assumptions used in this work, the predicted mass deposition of contaminant to the surface in the vicinity of the M2020 is relatively low. In terms of a localized predicted peak deposition, Fig 24 shows a localized maximum value of ~ 6 ng/(cm^2·sol). If a Mars surface wind maintained the same velocity, mean angle, and relatively narrow direction variance continuously for 100 sols, then a maximum of 6 ng of organic contaminant could accumulate on a potential sampling site (assuming 1 cm^2). This is only 4% of the original 150 ng contaminant budget per cached sample, and can easily be accommodated in the overall contaminant budget.

Furthermore, a strong diurnal effect is expected to be seen with wind direction, and the wind is expected to change by ~ 180° between a Martian day and night. This would generate a bi-modal wind direction distribution, further

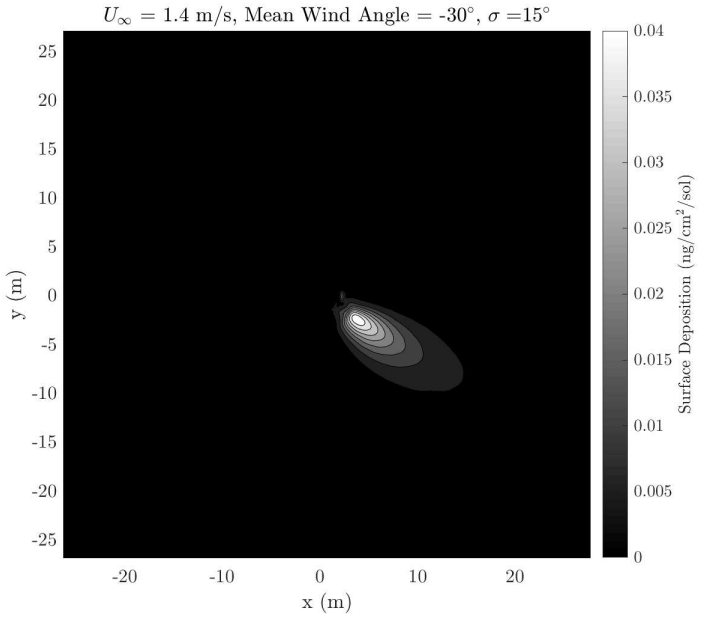

Fig. 21 Spatially averaged predicted contaminant surface mass deposition contour plot for $U(z_{ref})$ = 1.4 m/s, $\xi = -30°$, and $\sigma = 15°$.

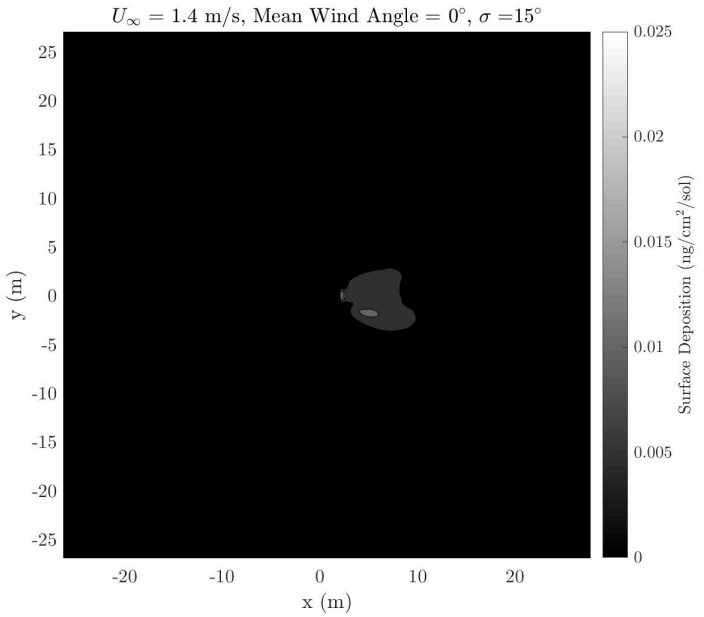

Fig. 22 Spatially averaged predicted contaminant surface mass deposition contour plot for $U(z_{ref})$ = 1.4 m/s, $\xi = 0°$, and $\sigma = 15°$.

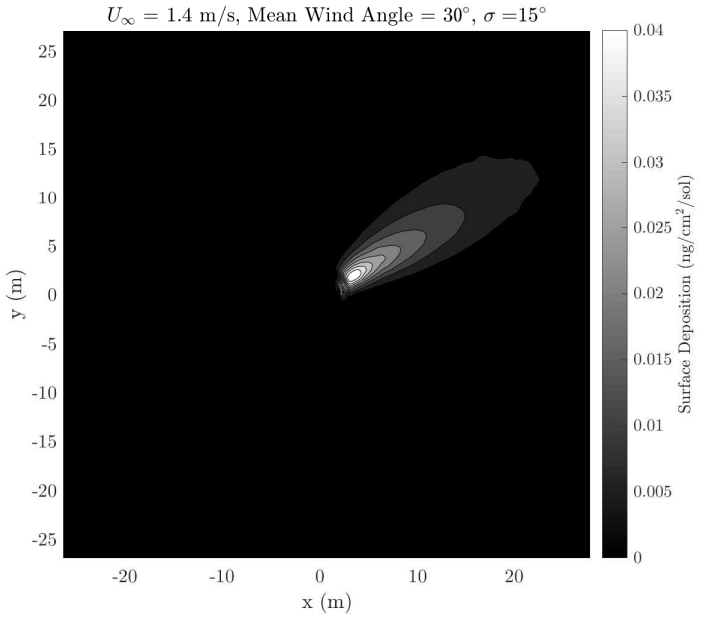

Fig. 23 Spatially averaged predicted contaminant surface mass deposition contour plot for $U(z_{ref})$ = 1.4 m/s, ξ = 30°, and σ = 15°.

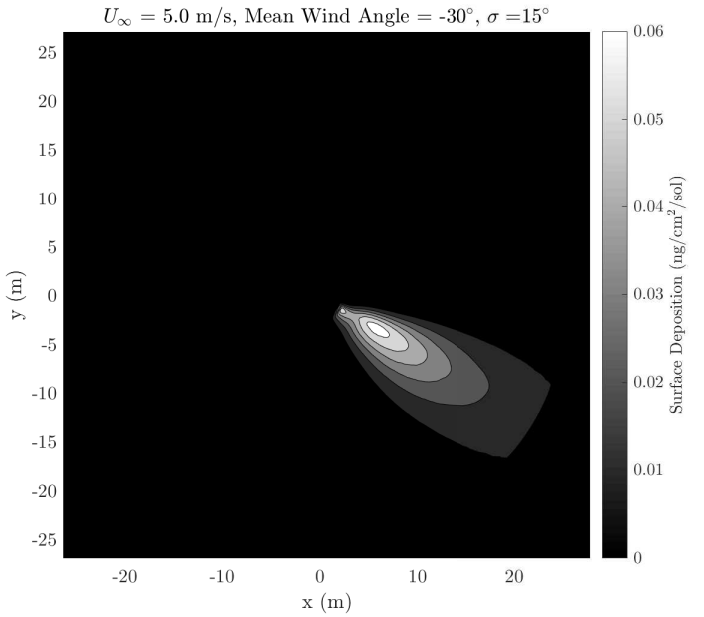

Fig. 24 Spatially averaged predicted contaminant surface mass deposition contour plot for $U(z_{ref})$ = 5.0 m/s, ξ = −30°, and σ = 15°.

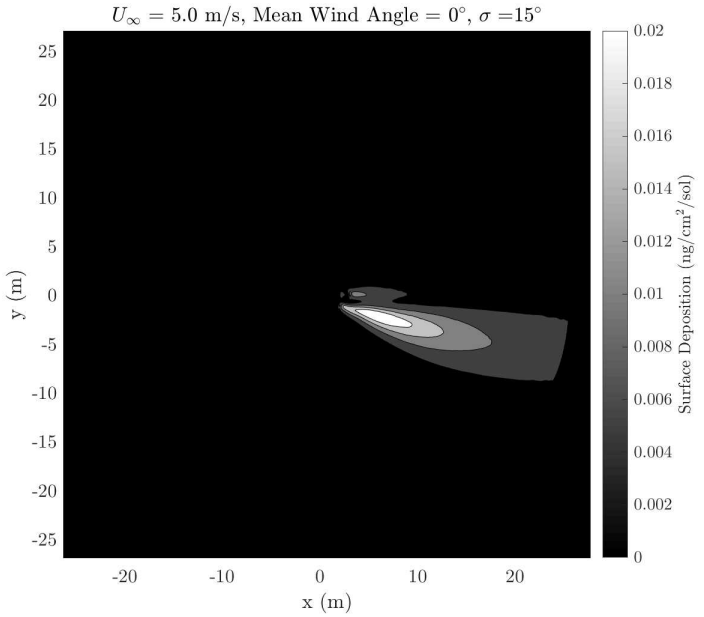

Fig. 25 Spatially averaged predicted contaminant surface mass deposition contour plot for $U(z_{ref})$ = 5.0 m/s, ξ = 0°, and σ = 15°.

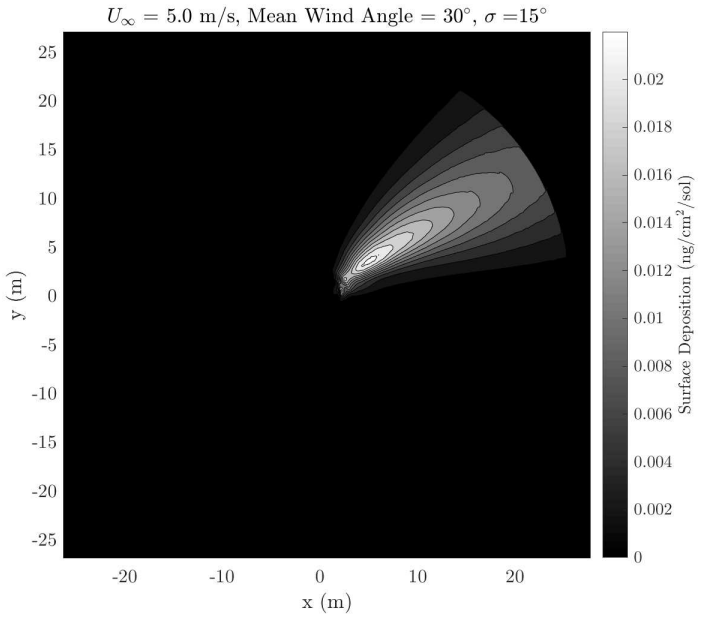

Fig. 26 Spatially averaged predicted contaminant surface mass deposition contour plot for $U(z_{ref})$ = 5.0 m/s, ξ = 30°, and σ = 15°.

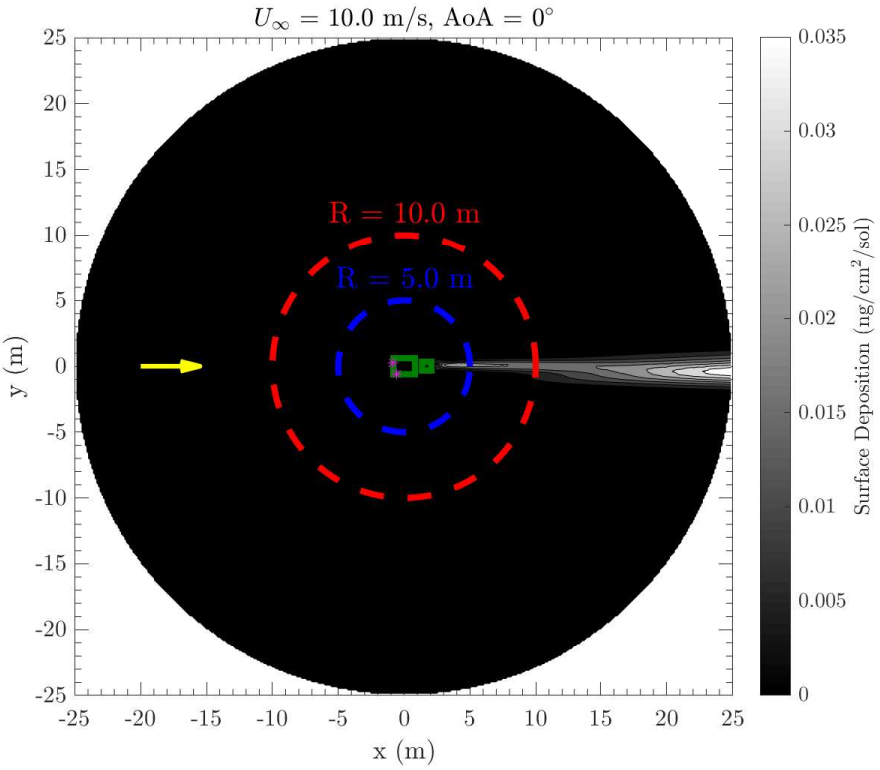

Fig. 27 Predicted contaminant surface mass deposition contour plot for $AoA = 0°$ and $U(z_{ref}) = 10.0$ m/s. The free-stream direction is shown by the yellow arrow, and an approximate outline of the rover and turret is shown in green (with vents noted). Circles showing 5 m and 10 m distances from the origin are shown for scale.

reducing the predicted contaminant mass deposition in the areas downstream of the rover. It is expected that local topography will have a large effect on the preferential wind direction experienced by the rover at a specific location, but a standard deviation of 15° is a small change in angle when compared to many of the MSL measurements [5]. If σ is increased, than the predicted contaminant deposition is expected to decrease linearly with σ.

The results presented used a binary diffusion coefficient for C_5H_{12} under Martian conditions. Using [13], D can be easily calculated for linear alkanes of C_4H_{10}–C_9H_{10} under Martian conditions. Using a simple exponential fit for D gives the relation $D = 0.0071 \cdot M_w^{-0.594}$, where M_w is the molecular weight of the species being considered in AMU, and the other two constants are consistent with D having units of m^2/s. The larger the hydrocarbon, the lower the binary diffusion coefficient. Decreasing the value of D used in the numerical simulations will decrease the predicted surface deposition of contaminant, as the first term in Eq. 2 is proportional to D.

While results for only two characteristic free-stream velocities have been presented in detail in this work, Fig. 27 shows the predicted contaminant deposition for $AoA = 0°$ and a characteristic free-stream velocity of 10 m/s. As the mesh was not changed for this simulation, increasing $y+$ values make it difficult to resolve all boundary layers. However, a significant reduction in contaminant deposition is observed in the domain when compared to Fig. 17, indicating that the increased free-stream velocity is convecting the contaminant farther downstream, and out of the area of interest before being potentially deposited on the surface. If desired, it would be possible to combine simulation results performed with different free-stream velocities and interpolating between them assuming a Weibull distribution for wind velocity, which has been used in the past [16, 17].

VI. Conclusions

A variety of numerical simulations were run to investigate the possibility of a molecular contaminant from the M2020 Rover WEB contaminating a potential sampling site in the vicinity of the rover. The molecular contaminant

was modeled numerically as a passive scalar, and a spatial averaging process was used to conservatively account for some of the wind variability expected to occur on the surface of Mars. Even considering potentially long rover loiter times on Mars (50 sols for the turret within 0.5 m of a potential sampling site, and 100 sols for the turret within 10 m of a potential sampling site), the predicted contaminant deposition values are well within acceptable levels, and do not constitute a major component of the 150 ng/sample requirement accepted by the M2020 mission.

Acknowledgments

The research was carried out at the Jet Propulsion Laboratory, California Institute of Technology, under a contract with the National Aeronautics and Space Administration. The authors would like to acknowledge the support of Eddie Ketsiri, for CAD support, and Carlee Wagner (Siemens) for STAR-CCM+ support.

References

[1] Summons, R., Sessions, A., Allwood, A., Barton, H., Beaty, D., Blakkolb, B., Canham, J., Clark, B., Dworkin, J., Lin, Y., Mathies, R., Milkovich, S., and Steele, A., "Planning Considerations Related to the Organic Contamination of Martian Samples and Implications for the Mars 2020 Rover," *Astrobiology*, Vol. 14, No. 12, 2014, pp. 969–1027. doi:https://doi.org/10.1089/ast.2014.1244, URL https://doi.org/10.1089/ast.2014.1244. 1

[2] Blakkolb, B., Logan, C., Jandura, L., Okon, A., Anderson, M., Katz, I., Aveni, G., Brown, K., Chung, S., Ferraro, N., Limonadi, D., Melko, J., Mennella, J., and Yavrouian, A., "Organic cleanliness of the Mars Science Laboratory sample transfer chain," *Review of Scientific Instruments*, Vol. 85, No. 7, 2014, p. 075111. doi:10.1063/1.4890279, URL https://doi.org/10.1063/1.4890279. 2

[3] Hess, S. L., Henry, R. M., Leovy, C. B., Ryan, J. A., and Tillman, J. E., "Meteorological results from the surface of Mars: Viking 1 and 2," *Journal of Geophysical Research*, Vol. 82, No. 28, 1977, pp. 4559–4574. doi:10.1029/JS082i028p04559, URL http://dx.doi.org/10.1029/JS082i028p04559. 2

[4] Murphy, J. R., Leovy, C. B., and Tillman, J. E., "Observations of Martian surface winds at the Viking Lander 1 Site," *Journal of Geophysical Research: Solid Earth*, Vol. 95, No. B9, 1990, pp. 14555–14576. doi:10.1029/JB095iB09p14555, URL http://dx.doi.org/10.1029/JB095iB09p14555.

[5] Newman, C. E., Gómez-Elvira, J., Marin, M., Navarro, S., Torres, J., Richardson, M. I., Battalio, J. M., Guzewich, S. D., Sullivan, R., de la Torre, M., Vasavada, A. R., and Bridges, N. T., "Winds measured by the Rover Environmental Monitoring Station (REMS) during the Mars Science Laboratory (MSL) rover's Bagnold Dunes Campaign and comparison with numerical modeling using MarsWRF," *Icarus*, Vol. 291, 2017, pp. 203 – 231. doi:https://doi.org/10.1016/j.icarus.2016.12.016, URL http://www.sciencedirect.com/science/article/pii/S0019103516304699. 2, 15, 19

[6] Dimotakis, P. E., "The mixing transition in turbulent flows," *Journal of Fluid Mechanics*, Vol. 409, 2000, p. 69–98. doi:10.1017/S0022112099007946. 3

[7] Holzer, M., and Siggia, E. D., "Turbulent mixing of a passive scalar," *Physics of Fluids*, Vol. 6, No. 5, 1994, pp. 1820–1837. doi:10.1063/1.868243, URL https://doi.org/10.1063/1.868243.

[8] Shraiman, B. I., and Siggia, E. D., "Scalar turbulence," *Nature*, Vol. 405, No. 6787, 2000, p. 639. doi:10.1038/35015000, URL http://dx.doi.org/10.1038/35015000.

[9] Warhaft, Z., "Passive Scalars in Turbulent Flows," *Annual Review of Fluid Mechanics*, Vol. 32, No. 1, 2000, pp. 203–240. doi:10.1146/annurev.fluid.32.1.203, URL https://doi.org/10.1146/annurev.fluid.32.1.203. 3

[10] Novak, K. S., Kempenaar, J. G., Redmond, M. J., and Bhandari, P., "Preliminary surface thermal design of the Mars 2020 Rover," *45th International Conference on Environmental Systems, ICES-2015-134*, Bellevue, Washington, 2015. 5

[11] Novak, K. S., Kempenaar, J., Liu, Y., Bhandari, P., and Lee, C.-J., "Thermal Performance of the Mars Science Laboratory Rover during Mars Surface Operations," *43rd International Conference on Environmental Systems, AIAA 2013-3322*, 2013. 5

[12] Cucullu, G. C., Zayas, D., Novak, K., and Wu, P., "A curious year on Mars—long-term thermal trends for Mars Science Laboratory Rover's first Martian year," *44th International Conference on Environmental Systems, ICES-2014-295*, 2014. URL https://ttu-ir.tdl.org/ttu-ir/handle/2346/59520. 5

[13] Bird, R. B., Stewart, W. E., and Lightfoot, E. N., *Transport Phenomena*, John Wiley & Sons, 1960. 6, 19

[14] Mahaffy, P. R., Webster, C. R., Atreya, S. K., Franz, H., Wong, M., Conrad, P. G., Harpold, D., Jones, J. J., Leshin, L. A., Manning, H., Owen, T., Pepin, R. O., Squyres, S., Trainer, M., and MSL Science Team, "Abundance and Isotopic Composition of Gases in the Martian Atmosphere from the Curiosity Rover," *Science*, Vol. 341, No. 6143, 2013, pp. 263–266. doi:10.1126/science.1237966, URL http://science.sciencemag.org/content/341/6143/263. 8

[15] Lienhard, J. H., *Synopsis of lift, drag, and vortex frequency data for rigid circular cylinders*, Vol. 300, Technical Extension Service, Washington State University, 1966. 8

[16] Lorenz, R. D., "Martian surface wind speeds described by the Weibull distribution," *Journal of Spacecraft and Rockets*, Vol. 33, No. 5, 1996, pp. 754–756. 19

[17] Lorenz, R. D., "Surface winds on Venus: Probability distribution from in-situ measurements," *Icarus*, Vol. 264, 2016, pp. 311 – 315. doi:https://doi.org/10.1016/j.icarus.2015.09.036, URL http://www.sciencedirect.com/science/article/pii/S0019103515004509. 19